

Evidence for an aspherical Population III supernova explosion inferred from the hyper metal-poor star HE 1327–2326*

RANA EZZEDDINE,^{1,2,3} ANNA FREBEL,^{2,1} IAN U. ROEDERER,^{4,1} NOZOMU TOMINAGA,^{5,6} JASON TUMLINSON,⁷
MIHO ISHIGAKI,⁸ KEN'ICHI NOMOTO,^{8,6} VINICIUS M. PLACCO,^{9,1} AND WAKO AOKI^{10,11}

¹*Joint Institute for Nuclear Astrophysics, Center for the Evolution of the Elements, East Lansing, MI 48824, USA*

²*Department of Physics and Kavli Institute for Astrophysics and Space Research,
Massachusetts Institute of Technology, Cambridge, MA 02139, USA*

³*Department of Physics and Astronomy, Michigan State University, East Lansing, MI 48824, USA*

⁴*Department of Astronomy, University of Michigan, Ann Arbor, MI 48109, USA*

⁵*Department of Physics, Faculty of Science and Engineering, Konan University, Kobe, Hyogo 658-8501, Japan*

⁶*Kavli Institute for the Physics and Mathematics of the Universe, The University of Tokyo, Kashiwa, Chiba 277-8583, Japan*

⁷*Space Telescope Science Institute, Baltimore, MD 21218, USA*

⁸*Department of Astronomy, School of Science, The University of Tokyo, Bunkyo-ku, Tokyo 113-0033, Japan*

⁹*Department of Physics, University of Notre Dame, Notre Dame, IN 46556, USA*

¹⁰*National Astronomical Observatory of Japan, Mitaka, Tokyo 181-8588, Japan*

¹¹*Department of Astronomical Science, The Graduate University for Advanced Studies, Mitaka, Tokyo 181-8588, Japan*

(Received November, 2018)

Submitted to ApJ

ABSTRACT

We present observational evidence that an aspherical supernova explosion could have occurred in the first stars in the early universe. Our results are based on the first determination of a Zn abundance in a *Hubble Space Telescope*/Cosmic Origins Spectrograph high-resolution UV spectrum of a hyper metal-poor (HMP) star, HE 1327–2326, with $[\text{Fe}/\text{H}](\text{NLTE}) = -5.2$. We determine $[\text{Zn}/\text{Fe}] = 0.80 \pm 0.25$ from a UV Zn I line at 2138 Å, detected at 3.4σ . Yields of a $25 M_{\odot}$ aspherical supernova model with artificially modified densities exploding with $E = 5 \times 10^{51}$ ergs best match the entire abundance pattern of HE 1327–2326. Such high-entropy hypernova explosions are expected to produce bipolar outflows which could facilitate the external enrichment of small neighboring galaxies. This has already been predicted by theoretical studies of the earliest star forming minihalos. Such a scenario would have significant implications for the chemical enrichment across the early universe as HMP Carbon Enhanced Metal-Poor (CEMP) stars such as HE 1327–2326 might have formed in such externally enriched environments.

Keywords: Galaxy: halo – nuclear reactions, nucleosynthesis, abundance – stars: abundances – stars: Population II – stars: supernovae – stars: individual (HE 1327–2326)

1. INTRODUCTION

Our knowledge on the nature, formation and properties of the Population III (Pop III) stars and their first supernova explosions (SNe) has been driven mainly by theoretical work and cosmological simulations (Bromm et al. 2009; Greif et al. 2010). These studies have, for example, predicted a large range of masses for the first stars over the past decade, from $<1 M_{\odot}$ to $>1000 M_{\odot}$ (Omukai & Palla 2001; Yoshida et al. 2006; Stacy et al. 2012; Hartwig et al. 2015). More generally, evidence on the first stars and SNe can be obtained from the chem-

Corresponding author: Rana Ezzeddine
ranae@mit.edu

* Based on observations made with the NASA/ESA Hubble Space Telescope, obtained at the Space Telescope Science Institute (STScI), which is operated by the Association of Universities for Research in Astronomy, Inc. (AURA) under NASA contract NAS 5-26555. These observations are associated with program GO-14151.

ical signatures of surviving low-mass, ultra metal-poor (UMP) stars with $[\text{Fe}/\text{H}]^1 < -4.0$ (Beers & Christlieb 2005). They likely formed from gas enriched by individual first SNe events whose chemical signature they have retained over billions of years (Frebel & Norris 2015; Hartwig et al. 2018).

Theoretical SNe nucleosynthesis yield calculations of Pop III progenitors have long been invoked to explain the origins of the observed abundance patterns in UMP stars (Woosley & Weaver 1995; Umeda & Nomoto 2002; Iwamoto et al. 2005; Tominaga et al. 2007b; Heger & Woosley 2010; Grimmett et al. 2018). Early spherical SNe models were not able to attain both the α -element and iron-peak (Mn, Co, Zn) abundance enhancements relative to iron (Cayrel et al. 2004), irrespective of the explosion energies employed (Woosley & Weaver 1995). Neither could they simultaneously produce the observed very large light element $[\text{C}, \text{N}, \text{O}/\text{Fe}] > 1$ ratios found in most UMP stars.

To better reproduce these ratios, a “mixing and fallback” (MF) SNe model was developed (Umeda & Nomoto 2002), defined by three parameters to account for aspherical effects, namely (i) the initial mass cut which corresponds to the inner boundary of the mixing region (M_{cut}), (ii) the outer boundary of the mixing region (M_{mix}), and (iii) the ejection factor (f) corresponding to the fraction of matter ejected from the mixed region. Two different mechanisms can be mimicked by the MF process (as shown in Figures 12 (a) and (b) in Tominaga et al. 2007b): (1) Faint, quasi-spherical MF SNe (with explosion energies $E \leq 10^{51}$ erg) which experience significant gravitational fallback of material onto the nascent black hole. Before the fallback, Rayleigh-Taylor instabilities induce mixing (Joggerst et al. 2010) of the products of complete silicon burning (e.g., calcium, titanium and iron) with material from the carbon-oxygen core. (2) Aspherical bipolar jet SNe which experience significant gravitational fallback of material onto the nascent black hole along the equatorial plane and ejection of material from the complete Si burning layers along the jets (Tominaga et al. 2007a; Tominaga 2009). Both mechanisms result in the ejection of a relatively small (residual) amount of iron but a comparably large amount of, e.g., carbon (Umeda & Nomoto 2002). This way, the large ratios of $[\text{C}/\text{Fe}]$, $[\text{N}/\text{Fe}]$, and $[\text{O}/\text{Fe}]$ in UMP stars could be produced.

The difference between the two mechanisms, however, appears in the abundance ratios among Fe-peak elements. In the former quasi-spherical faint explosion

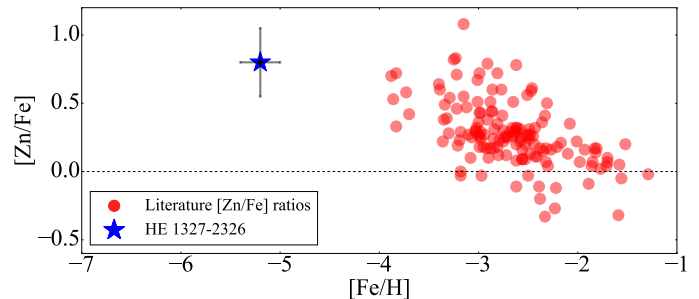


Figure 1. $[\text{Zn}/\text{Fe}]$ abundance ratios for metal-poor stars with $-4 < [\text{Fe}/\text{H}] < -1$ from Cayrel et al. (2004), Barklem et al. (2005), Hollek et al. (2011) and Jacobson et al. (2015). The $[\text{Zn}/\text{Fe}] = 0.80 \pm 0.25$ obtained in this work for HE 1327–2326 at $[\text{Fe}/\text{H}] = -5.20 \pm 0.20$ is shown by the blue star and black error bars. Abundance values are extracted from the JINAbase (Abohalima & Frebel 2018).

model, large Zn and other iron-peak elemental abundances cannot be obtained (Tominaga 2009; Nomoto et al. 2013; Grimmett et al. 2018) because a weak explosion energy is required to achieve the extensive fallback (necessary for producing a low iron abundance). On the other hand, in the aspherical bipolar jet explosion model, the high entropy environment along the jets enables large $[\text{Zn}/\text{Fe}]$ ratios since more Zn is ejected. Studies of extremely metal-poor stars with $-4.5 < [\text{Fe}/\text{H}] < -3$ have indeed shown enhanced $[\text{Zn}/\text{Fe}] > 0$ ratios (Figure 1; abundance data from Cayrel et al. 2004; Barklem et al. 2005; Hollek et al. 2011; Jacobson et al. 2015; abundances extracted from the JINAbase²; Abohalima & Frebel 2018), thus favoring the aspherical explosion model.

But no zinc measurements have thus far been possible for stars with $[\text{Fe}/\text{H}] < -4.5$ due to the intrinsic weakness of the strongest optical zinc triplet lines at 4680 Å, 4722 Å and 4810 Å. However, another strong Zn I line exists in the UV spectral range at 2138 Å. Unfortunately, all stars with $[\text{Fe}/\text{H}] < -4.5$ are much too faint for successful UV observations—with the exception of HE 1327–2326, a Milky Way halo hyper metal-poor (HMP) star with $[\text{Fe}/\text{H}](\text{NLTE}) = -5.2$ (Ezzeddine & Frebel 2018). This star has been extensively studied based on optical spectra (Frebel et al. 2005; Aoki et al. 2006; Frebel et al. 2008; Korn et al. 2009). To continue to provide the most stringent observational constraints on the explosion mechanism, the details of the progenitor star and the origin of Zn in UMP stars, we obtained a *Hubble Space Telescope*/Cosmic Origins Spectrograph (*HST*/COS) high-resolution UV spectrum for

¹ Defined as $[A/B] = \log_{10}(N_A/N_B)_{\text{star}} - \log_{10}(N_A/N_B)_{\odot}$, with N_A and N_B being the respective elements number densities.

² <https://jinabase.pythonanywhere.com>

HE 1327–2326 in which we detected the absorption line of zinc at 2138 Å for the first time.

We describe the UV observations and data reduction in Section 2 and the chemical abundance analysis in Section 3. We use the [Zn/Fe] ratio in HE 1327–2326 to constrain the SNe properties of its first star progenitor in Section 4, and present our interpretations and conclusions in Section 5.

2. OBSERVATIONS AND DATA REDUCTION

We obtained UV observations of HE 1327–2326 with the Cosmic Origins Spectrograph (COS) on board the *Hubble Space Telescope (HST)* (Program ID: GO-14151), during May 07-15 2016. The spectrum covers the three wavelength regions: 2118 – 2151 Å, 2216 – 2249 Å and 2315 – 2348 Å. The total integration time was 22 hrs and 20 minutes. We performed a custom data reduction to optimize the signal-to-noise (S/N) ratio of the final spectrum. By default, the COS extraction pipeline, CALCOS (Fox et al. 2015), uses an extraction box height of 56 pixels in the cross dispersion (“y”) direction to extract the three stripes from the exposures. This procedure ensures that virtually all the source flux is captured, but at the cost of summing over pixels where the raw S/N is very low. Alternatively, we used an extraction box height of 9 pixels in the cross dispersion direction. This height collects somewhat less than the total source flux (at the 10% level) and so can be used safely for line-to-continuum contrast measurements but not for cases where precise spectro-photometric measurements are necessary for the science. In our case, the vertical (cross-dispersion or “y”) location of the 9-pixel extraction boxes was tuned individually for each stripe in each exposure using the B.SPEC and HEIGHT parameters in the XTRACTAB reference file, and the edge-to-edge slope (SLOPE) in the diagonal boxes was retained at their default values. This is the procedure recommended by the STScI COS instrument team (Snyder & Sonnentrucker 2017). More details on the extraction, co-addition and normalization of the final UV spectrum can also be found in Ezzeddine & Frebel (2018).

One Zn I line at 2138.57 Å, five Fe II lines and one Si I line, were detected in the final UV spectrum. Figure 2 shows parts of these detections. For visual purposes, the bottom right panel (f) of Figure 2 shows the Zn I line region smoothed with an average boxcar of a 2 pixels width. The abundances of Fe and Si were determined and discussed further in Ezzeddine & Frebel (2018).

3. CHEMICAL ABUNDANCE ANALYSIS

3.1. Fundamental Stellar Parameters

In our abundance analysis of HE 1327–2326, we use an effective temperature of $T_{\text{eff}} = 6180 \pm 80$ K, derived from color-effective temperature relations using broadband *UBVRI* photometry (Frebel et al. 2005), a surface gravity of $\log g = 3.7 \pm 0.2$ and a microturbulent velocity of $\xi_t = 1.7 \text{ km s}^{-1}$ based on previous studies (Korn et al. 2009; Ezzeddine & Frebel 2018). The *Gaia* second data release DR2 (Gaia Collaboration et al. 2018) produced $T_{\text{eff}} = 5915 \pm 300$ K and $\log g = 3.40 \pm 0.3$ based on photometric colors and parallax, respectively. We use both sets of stellar parameters to determine the [Zn/Fe] abundance ratio of HE 1327–2326. We employ a standard model atmosphere (Castelli & Kurucz 2004) with input model metallicity of [Fe/H] = −5.0 and α -enhancement [α /Fe] = 0.4 throughout.

3.2. [Zn/H] and [Zn/Fe] abundances in HE 1327–2326

We measure an equivalent width of 43.4 ± 12.7 mÅ for the Zn I line at 2138.57 Å, by convolving the COS line-spread functions (Ghavamian et al. 2009) with Gaussian profiles following Roederer et al. (2016). We determine uncertainties in the equivalent width and Zn abundance measurements by altering the continuum placement and the full-width half maximum (FWHM) of the spectral line by $\pm 1 \sigma$, and recording the corresponding changes. We assess a detection significance of 3.4σ by dividing the equivalent width of the line by its uncertainty. We then calculate the abundance of Zn using the equivalent width curve-of-growth method using the Local Thermodynamic Equilibrium (LTE) radiative transfer code MOOG updated to include proper scattering treatment (Snedden 1973; Sobeck et al. 2011), and with custom analysis tools (Casey 2014). The abundances are determined relative to the solar values from Asplund et al. (2009).

Using $T_{\text{eff}} = 6180$ K and $\log g = 3.7$ (Frebel et al. 2008), we determine a Zn abundance of [Zn/H] = -4.40 ± 0.25 using the 1D, LTE framework. Conditions of line formation in metal-poor stars are known to deviate from the assumptions of LTE and 1D model atmospheres (Thévenin & Idiart 1999; Mashonkina et al. 2011; Bergemann et al. 2012; Takeda et al. 2005). Abundances from lines of minority species, such as neutral Zn I and Fe I, are often prone to larger non-local thermodynamic equilibrium (NLTE) effects in the atmospheres of low metallicity stars than from line of the corresponding dominant ionized species. Investigations of possible NLTE effects for abundances of commonly used optical Zn I lines over a range of stellar parameters showed that NLTE abundance corrections, defined by the differences between the NLTE and LTE abundances using the same observed equivalent widths, are actually not

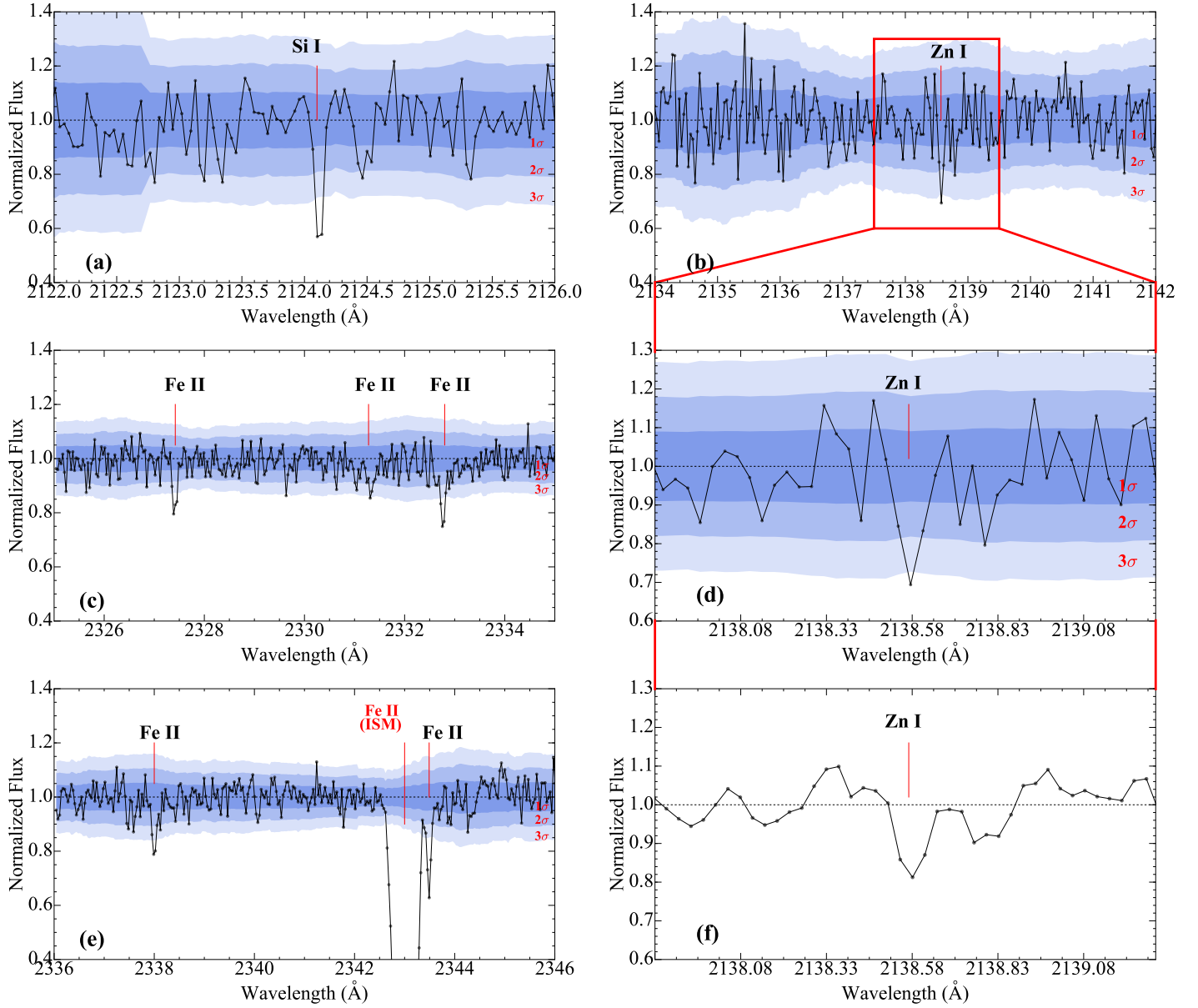


Figure 2. Selected regions of the co-added UV spectrum of HE 1327–2326, where atomic lines of Si I, Zn I and Fe II were detected for the first time. The Fe II interstellar medium (ISM) line at 2343 Å is also detected, as shown in panel (e). The detection significance levels of the lines are shown by the different shaded areas: 1σ (darkest blue), 2σ (light blue) and 3σ (lightest blue). For clarification purposes, panel (f) shows a smoothed part of the spectrum centered around the Zn line at 2138.57 Å, and covering the same spectral range as panel (d). The spectrum was smoothed using an average boxcar smoothing with a 2.0 pixel width. For completeness, we also show the Si I and Fe II spectral line regions, studied in details in [Ezzeddine & Frebel \(2018\)](#).

Table 1. Chemical abundances of 13 elements determined from the UV and optical spectra of HE 1327–2326. Upper limits for Sc, Mn and Co are also included.

El	N_{nlines}	$\log \epsilon(X)$	$\sigma \log \epsilon(X)$	[X/H]	[X/Fe]
C (CH)	syn.	6.21 ^a	0.10	−2.22	3.49
N (NH)	syn.	6.10 ^a	0.20	−1.73	3.98
O (OH)	syn.	6.12 ^a	0.20	−2.57	3.14
Na I	2	2.99	0.04	−3.25	2.46
Mg I	4	3.54	0.02	−4.06	1.65
Al I	1	1.90	0.03	−4.55	1.16
Si I ^b	1	2.80	0.27	−4.71	1.28
Ca II	4	1.34	0.15	−5.00	0.71
Ti II	15	−0.09	0.17	−5.04	0.67
Fe I ^c	10	1.79	0.15	−5.71	...
Fe I ^d	10	2.30	0.11	−5.20	...
Fe II	4	1.51	0.26	−5.99	...
Ni I	4	0.73	0.20	−5.49	0.33
Zn I	1	+0.16	0.25	−4.40	0.80
Sr II	2	−1.76	0.06	−4.63	1.08
Sc II	< −1.68	...	< −4.83	< 0.88
Mn I	< 0.53	...	< −4.90	< 0.81
Co I	< 0.58	...	< −4.41	< 1.30

^a3D values adopted from Frebel et al. (2008)

^bAdopted from Ezzeddine & Frebel (2018)

^cLTE abundance from Frebel et al. (2008)

^dNLTE abundance adopted from Ezzeddine & Frebel (2018)

significant and ≤ 0.2 dex (Takeda et al. 2005). Even though the departures from LTE have not been calculated explicitly for any UV Zn I lines, it could be shown by Roederer & Barklem (2018) that ionization equilibrium in LTE can be reached in metal-poor stars with $-3.0 < [\text{Fe}/\text{H}] < -1.0$ (within 0.1 dex) using optical (e.g., Zn I $\lambda 4810$) and UV (e.g., Zn II $\lambda 2062$) lines. Departures from LTE for Zn were indeed insignificant, even at $[\text{Fe}/\text{H}] = -3.0$. Following these results, we assume that our LTE Zn abundance, as derived from the UV line, would be compatible with values obtained from any optical lines, if ever detected.

For Fe, however, strong NLTE effects have been well documented (e.g., Asplund 2005, and references therein). We thus adopt the 1D, NLTE Fe abundance of $[\text{Fe}/\text{H}] = -5.20$ in HE 1327–2326, inferred from 10 Fe I optical lines as determined in Ezzeddine & Frebel (2018). This Fe abundance for HE 1327–2326 is based on detailed investigations of possible 3D and NLTE effects on both Fe I and Fe II lines in the optical and UV.

We then obtained a zinc to iron abundance ratio of $[\text{Zn}/\text{Fe}] = 0.80 \pm 0.25$. For completeness, we note that any potential NLTE correction to the Zn I abundance (should they exist) would be positive, and would thus only further increase the $[\text{Zn}/\text{Fe}]$ ratio (Takeda et al. 2005).

We also investigate the $[\text{Zn}/\text{Fe}]$ abundance ratio using the *Gaia* DR2 stellar parameters which yield slightly lower 1D, LTE Zn and 1D, NLTE Fe abundances of $[\text{Zn}/\text{H}] = -4.70$ and $[\text{Fe}/\text{H}] = -5.40$, respectively. This 1D, NLTE abundance of Fe was determined following the same setup used in Ezzeddine et al. (2017). Compared to our other value, the $[\text{Zn}/\text{Fe}]$ decreases only slightly, to 0.70 ± 0.25 . This shows that the $[\text{Zn}/\text{Fe}]$ ratio in HE 1327–2326 is robustly enhanced, irrespective the choice of stellar parameters.

To establish the overall $[\text{X}/\text{Fe}]$ abundance pattern of HE 1327–2326, we adopt $[\text{Zn}/\text{Fe}] = 0.80 \pm 0.25$, in addition to the UV Si I abundance from Ezzeddine & Frebel (2018) as well as the optical abundances for 11 elements and upper limits for five others (Sc, V, Cr, Mn and Co) from Frebel et al. (2008). All elemental abundances used are listed in Table 1. We use this pattern to compare to the theoretical SNe nucleosynthesis yields of various models.

4. CONSTRAINING THE POP III STAR EXPLOSION PROPERTIES

4.1. Comparison to faint mixing and fallback quasi-spherical SNe models

Previous studies have commonly compared abundance patterns of individual UMP stars, such as that of HE 1327–2326, to the yields of faint mixing and fallback quasi-spherical Pop III SNe (Umeda & Nomoto 2002; Iwamoto et al. 2005; Frebel et al. 2005; Christlieb et al. 2004; Keller et al. 2014; Bessell et al. 2015; Placco et al. 2016; Nordlander et al. 2017). As discussed in Section 1, such type of spherical explosion underproduces iron peak elements (such as Co, Cr, or Zn) (Tominaga 2009; Grimmett et al. 2018; Hirai et al. 2018; Tsujimoto & Nishimura 2018). Due to a lack of iron peak abundances, the comparisons of the data with these model results usually remained unconstrained in the that region. With available Zn abundances, however, new constraints can be obtained.

We perform statistical fitting tests following Placco et al. (2016), to compare the determined abundance pattern of HE 1327–2326 (including Zn) to 16,800 theoretical yields³ of quasi-spherical mixing and fallback SNe

³ Models from <https://2sn.org/starfit/> (Heger & Woosley 2010)

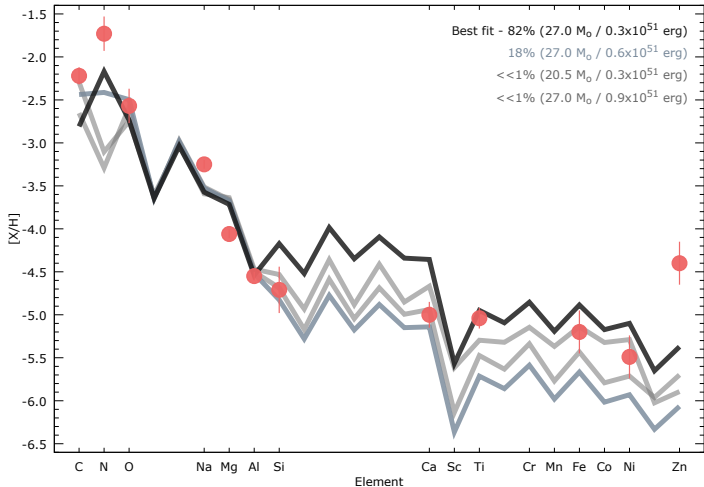


Figure 3. Statistical results for comparisons of a large grid of (16,800) mixing and fallback (quasi-spherical) SNe nucleosynthesis yields (Heger & Woosley 2010) with different progenitor masses and explosion energies, to 10,000 re-sampled chemical abundance patterns of HE 1327–2326.

models, computed with different explosion parameters (e.g., progenitor mass, explosion energies, mixing parameters). To account for uncertainties in our fitting results, we simulate 10,000 different abundances for each observed element used in the fit, which follow a normal distribution centered around the measured abundance (taken as the mean). We then randomly sample the abundance distributions for all elements and generate 10,000 artificial abundance patterns for HE 1327–2326, to compare the yields. Our results, shown in Figure 3, demonstrate that indeed none of the mixing-fallback supernova models can match the Zn abundance (relative to Fe) in HE 1327–2326. Overall, 82% of the simulated abundance patterns of HE 1327–2326 can be fit best (although not satisfactorily) with a $27 M_{\odot}$ progenitor exploding with 0.3×10^{51} erg. 18% of the simulated abundance patterns are also reproduced by a $27 M_{\odot}$ progenitor, but with a slightly higher explosion energy of 0.6×10^{51} erg. The remaining few abundance patterns ($\ll 1\%$) are fit best with $20.5 M_{\odot}$ and $27 M_{\odot}$ progenitors with 0.3×10^{51} ergs and 0.9×10^{51} ergs, respectively.

Building on these results, we can statistically rule out faint quasi-spherical SNe as the source of metals in HE 1327–2326, as no superposition of yields would produce enough Zn relative to the lighter elements. Enrichment by multiple events can also more broadly be eliminated following the theoretical mono-enrichment classification scheme suggested by Hartwig et al. (2018), in which stars with $-6.0 < [\text{Fe}/\text{H}] < -4.0$ and $[\text{Mg}/\text{C}] < -1.0$ have a strong likelihood of being enriched by a single SNe event. This applies well to HE 1327–2326

with $[\text{Fe}/\text{H}] = -5.2$ and $[\text{Mg}/\text{C}] = -1.84$. Overall, this shows that the progenitor of HE 1327–2326, and possibly those of other UMP stars with similar abundance patterns, did not explode (quasi-)spherically.

4.2. Comparison to Aspherical SNe models

We compare the abundance pattern of HE 1327–2326 to the yields of artificially density modified mixing and fallback models with different masses and explosion energies, thus mimicking aspherical SNe with bipolar outflows. Specific details on the explosion models and yield calculations are described in Tominaga et al. (2007b). We find that the yields of a $25 M_{\odot}$ first star progenitor exploding with an aspherical SNe, with a high explosion energy of $E = 5 \times 10^{51}$ ergs best matches the entire abundance pattern of HE 1327–2326, including zinc. We show this result by the black solid line in Figure 4. Our best fit model has an initial mass cut of $M_{\text{cut}} = 1.64 M_{\odot}$, outer boundary mixing region mass of $M_{\text{mix}} = 5.65 M_{\odot}$ and an ejection factor of $f = 0.0002$. To increase specifically the zinc yield of a mixing and fallback SNe model, the explosion mechanism was modified such that the matter density is artificially reduced, to mimic a high entropy explosion environment, which is required for increased explosive nucleosynthesis (Maeda & Nomoto 2003; Tominaga et al. 2007a,b; Grimmett et al. 2018). In this modified framework, elements formed in the deepest layers during the explosion, such as zinc, are (at least partially) mixed upward and then ejected. This occurs alongside the release of only small amounts of iron (most iron falls back onto the nascent black hole) and large amounts of, e.g., carbon made in the layers further out. The density artificially modified mixing and fallback model thus parameterizes what would physically be an aspherical SNe with bipolar outflows or jets (See panel (b) of Figure 12 in Tominaga et al. 2007b), with the ejection factor f in the 1D model being equivalent to the fraction of the solid angle of the region where the ejected mass elements in the Si-burning layer are located in the 2D model (i.e., $f = 1$ in the spherical model). The necessary high-entropy environment would occur along the rotation axis. Tominaga (2009) showed that the abundance patterns of the yields of the 2D aspherical bipolar explosion is reproduced by the density modified mixing and fallback model. Unfortunately, more realistic 3D explosion models of metal-free stars are not available yet to further investigate this behaviour.

We also explore other geometries using the same progenitor mass of $25 M_{\odot}$ including two quasi-spherical mixing and fallback SNe models with low ($E = 1 \times 10^{51}$ ergs; teal solid line in panel (a) of Figure 4) and high ($E = 5 \times 10^{51}$ ergs; magenta solid line in panel (a) of

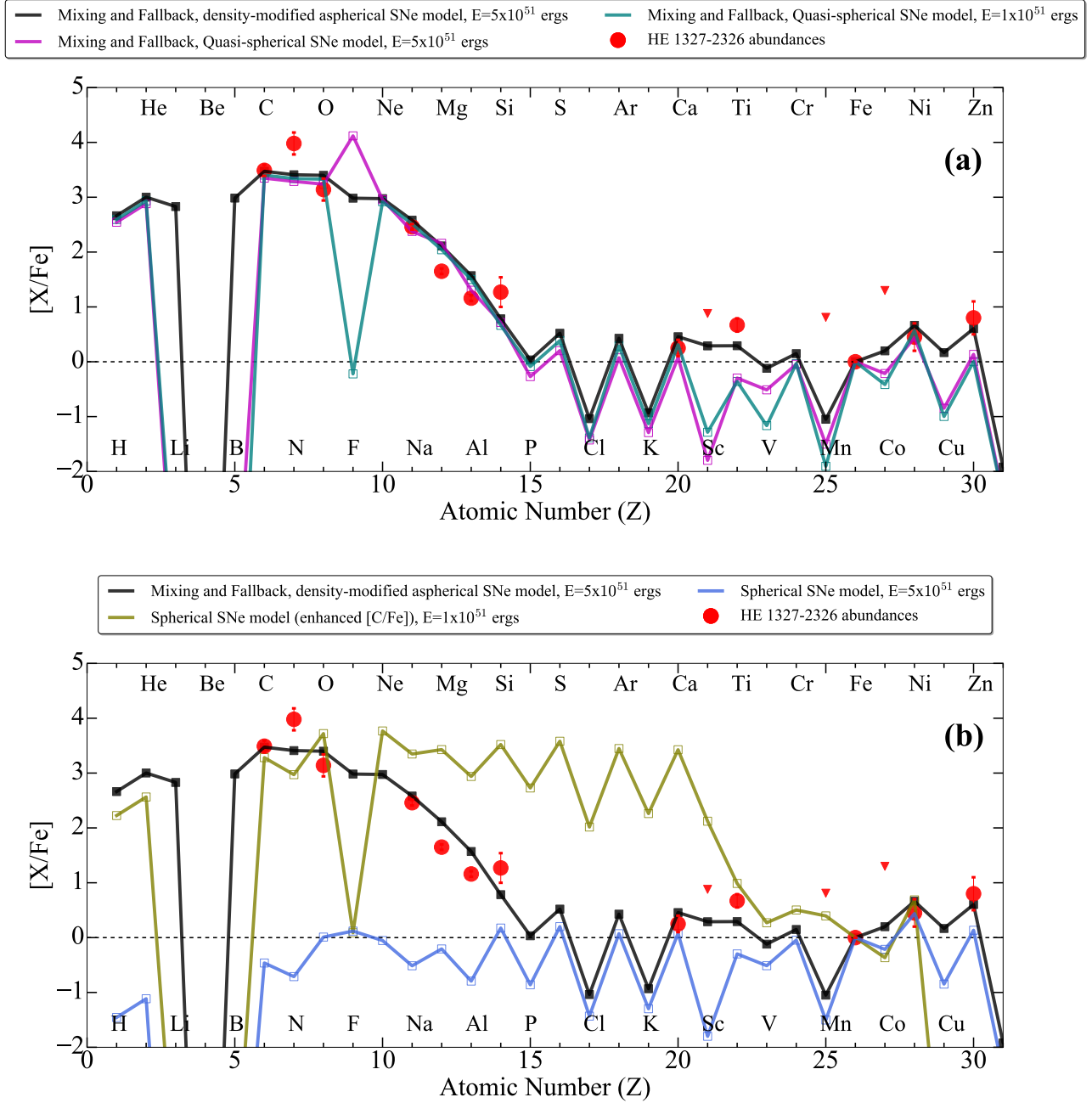


Figure 4. Best-fit yields of an artificially density-modified “mixing and fallback” mimicking an aspherical SNe explosion model with bipolar-outflows of a first star progenitor with $25 M_{\odot}$ and $E_{51} = 5 \times 10^{51}$ ergs explosion energy (black solid line). This is obtained from fitting various models and associated parameters to the measured abundance pattern of HE 1327–2326 (red symbols). Triangles indicate upper limits. Panel (a) also shows yields for two $25 M_{\odot}$ quasi-spherical mixing and fallback explosion models with explosion energies of $E = 1 \times 10^{51}$ ergs (solid teal line) and $E = 5 \times 10^{51}$ ergs (solid magenta line), respectively. Panel (b) shows yields for two spherical SNe explosion models with $E = 1 \times 10^{51}$ ergs and enhanced $[C/Fe]$ ratio (solid gold line), and $E = 5 \times 10^{51}$ ergs (solid blue line), respectively. Only the artificially density modified, aspherically mimicked model with bipolar jets is able to reproduce the largely enhanced $[Zn/Fe]$ abundance ratio determined in HE 1327–2326.

Figure 4) explosion energies. Two spherical SNe models with and without enhanced $[C/Fe]$ ratios were also explored corresponding to, respectively, the gold and blue solid lines in panel (b) of Figure 4. The explosion parameters M_{cut} , M_{mix} and f used for each of these models are listed in Table 2. Both quasi-spherical mixing and fallback models with $E = 1 \times 10^{51}$ ergs and $E = 5 \times 10^{51}$ ergs are not able to produce the $[Zn/Fe] > 0$ ratio. Simultaneously, they also under-reproduce the $[Sc/Fe]$ and $[Ti/Fe]$ ratios as compared to the aspherical model. The explosive nucleosynthesis in the density modified, high-entropy aspherical model enhances the α -rich freezeout, thus enhancing the $[Sc/Fe]$ and $[Ti/Fe]$ ratios usually determined in extremely metal-poor (EMP) stars with $[Fe/H] < -3$ (Tominaga et al. 2007b). Given that the determined $[Ti/Fe]=0.67$ ratio in HE 1327–2326 is enhanced, an aspherical explosion model is thus clearly favoured.

We note that spherical models could principally also produce a high entropy environment, and hence, a solar $[Zn/Fe]$ ratio if the explosion energy were large enough, e.g., $E = 5 \times 10^{51}$ ergs (see panel (b) of Figure 4) (Nomoto et al. 2013). However, such an energetic explosion would be highly inconsistent with the significant fallback required to produce the low Fe abundances observed in UMP stars, including HE 1327–2326. This explains why the spherical models are unlikely contenders for the explosion mechanisms of HE 1327–2326’s progenitor, and perhaps even for other first stars.

Overall, the explosion of the massive Pop III star progenitor of HE 1327–2326 is thus more energetic than previously thought (i.e., a hypernova), in line with more recent studies, such as Grimmer et al. (2018). Interestingly, previous work has suggested that only faint mixing and fallback first SNe would seed carbon-enhanced metal-poor (CEMP) stars such as HE 1327–2326, since their host minihalos would be disrupted by any larger energy input (Cooke & Madau 2014). Our results provide an alternative explanation, since high energy aspherical SNe explosions could also produce high $[C/Fe]$ ratios.

4.3. Evidence for aspherical explosions from rotation

It has been proposed that aspherical SNe are driven by (fast) rotating progenitors with possibly strong magnetic fields (Maeda & Nomoto 2003; Meynet et al. 2006; Ekström et al. 2008). This is in line with theoretical predictions that the first stars were heavily rotating (Meynet et al. 2006; Stacy et al. 2011; Tsujimoto & Nishimura 2018). Indeed, the progenitors of HE 1327–2326 and those of other second generation stars have already been shown to be fast rotating based

on their large relative nitrogen abundance ratios, e.g., $[N/Fe] = 3.98$ in HE 1327–2326, $[N/Fe] = 2.57$ in HE 0107–5240 (Christlieb et al. 2004), and $[N/Fe] = 3.46$ in SD 1313–0019 (Frebel et al. 2015).

Stellar surface nitrogen abundances become enhanced due to internal mixing caused by rotation (Meynet et al. 2006; Choplin et al. 2017), rather than being produced during their explosion (see Figure 4). Additionally, Maeder et al. (2015) and Choplin et al. (2018) have proposed that a fast rotating Pop III star progenitor could be responsible for the enhanced $[Sr/Fe]=1.08$ determined for HE 1327–2326 and other EMP stars with $[Sr/Fe] > 0.5$. They showed that fast rotation in a low-metallicity, massive star can set off a strong mixing between the H- and He-burning zones which triggers the synthesis of Sr and other light neutron-capture elements made in the s-process.

Introducing rotation of Pop III stars into the standard neutrino-driven paradigm of core-collapse supernovae has independently been shown to lead to bipolar (jet-like) SNe (Fryer & Heger 2000; Burrows et al. 2004). Finally, rotation has also been implemented into early universe and first stars cosmological simulations (Greif et al. 2010; Stacy et al. 2011) to investigate the ab-initio formation of the first stars. Moreover, Tsujimoto & Nishimura (2018) recently predicted through their galactic chemical evolution calculations that magneto-rotational driven explosions could indeed be the dominant source of enhanced $[Zn/Fe]$ abundance ratios in the Milky Way satellite dwarf galaxy stars with $-4 < [Fe/H] < -1$.

4.4. νp -process in SNe: Is it able to produce the enhanced $[Zn/Fe]$ in HE 1327–2326?

Fröhlich et al. (2006a) and Pruet et al. (2006) proposed that increasing the entropy by increasing the electron mole fractions Y_e in a faint quasi-spherical SNe model to values > 0.5 would mimic a νp -process in the neutrino driven winds emerging from the proto-neutron star of the Pop III progenitor. This could enhance the production of $[Sr/Fe]$ as well as the iron peak elements $[Sc, Co, Zn/Fe]$ ratios, as is observed in UMP stars.

Fröhlich et al. (2006b), however, showed that such a scenario only leads to the production of Zn of up to $[Zn/Fe] = 0$ which remains inconsistent with observational results of $[Zn/Fe] \gtrsim 0.5$, as determined for EMP stars and HE 1327–2326. Tominaga et al. (2007b) confirmed these results by introducing neutrino-transport into their mixing and fallback SNe models of Pop III stars by artificially increasing Y_e in the complete Si burning region where Zn is produced. They showed that increasing Y_e to > 0.5 could indeed enhance the pro-

Table 2. Parameters of the different SNe model yields used in Figure 4.

Model	Mass	E	M_{cut}	M_{mix}	f
	$[M_{\odot}]$	$[10^{51} \text{ ergs}]$	$[M_{\odot}]$	$[M_{\odot}]$	
Mixing and Fallback, density-modified aspherical	25	5	1.64	5.65	0.0002
Mixing and Fallback, quasi-spherical, high energy	25	5	1.59	5.69	0.0001
Mixing and Fallback, quasi-spherical, low energy	25	1	1.61	5.65	0.00015
Spherical, enhanced [C/Fe]	25	1	2.24	...	1
Spherical	25	5	1.59	...	1

duction of $[\text{Sc}/\text{Fe}] > 0.3$ as is observed in EMP stars but could not simultaneously produce the enhanced $[\text{Zn}/\text{Fe}] > 0$ as well as $[\text{Co}/\text{Fe}] > 0$.

This suggests that the νp process is not responsible for the enhanced Zn production in HE 1327–2326 and other EMP stars. Instead, the entire abundance pattern of HE 1327–2326 can be produced by rotation-driven, high energy ($E = \times 10^{-51}$ ergs) aspherical SNe with bipolar-jets, as described in Sections 4.2 and 4.3. Nevertheless, the νp process could contribute to an increased $[\text{Sr}/\text{Fe}]$ ratio as has been determined for HE 1327–2326 and other UMP stars.

5. INTERPRETATION AND CONCLUSIONS: EVIDENCE FOR EXTERNAL CHEMICAL ENRICHMENT

Stellar abundance trends of various elements show increasing amounts of scatter with decreasing iron abundance. The fraction of stars with unusual abundance patterns is the highest at the lowest $[\text{Fe}/\text{H}]$, with $\sim 80\%$ for $[\text{Fe}/\text{H}] < -4.0$, including HE 1327–2326. This has previously been interpreted as a result of inhomogeneous metal mixing or unusual SNe at the earliest times (Frebel & Norris 2015). On the contrary, the vast majority of metal-poor stars with $[\text{Fe}/\text{H}] > -4.0$ show patterns generally in line with a formation from well mixed gas (Cayrel et al. 2004; Yong et al. 2013). It is thus possible that these different types of abundance patterns are the result of different chemical enrichment channels that could have operated in the early universe. If one channel was common and the other rare, it might explain the extreme rarity of stars with $[\text{Fe}/\text{H}] < -4.5$ which remain to have a poorly understood origin scenario. This idea is principally supported by the fact that models for metallicity ($[\text{Fe}/\text{H}]$) distribution function cannot reproduce the existence of the low- $[\text{Fe}/\text{H}]$ tail with $[\text{Fe}/\text{H}] < -4.0$ (Yong et al. 2013) simultaneously with the body of data on metal-poor stars with higher $[\text{Fe}/\text{H}]$ abundances.

These challenges might be explained by the existence of aspherical Pop III SNe, as described in this work. The ejecta structure of a bipolar explosion is different than that of a quasi-spherical explosion, in that the high energy bipolar explosion produces high velocity ejecta along the polar axis as well as along the equatorial plane. These velocities can reach up to $4 \times 10^4 \text{ km s}^{-1}$ and $8 \times 10^3 \text{ km s}^{-1}$ after 50 s of the explosion, respectively (Tominaga 2009). This is higher than what can be maximally produced by faint mixing-fallback explosions ($4 \times 10^3 \text{ km s}^{-1}$) (Iwamoto et al. 2005). A high-velocity ejecta could facilitate carrying the SNe yields out of the parent host minihalo to enrich a neighboring minihalo. Theoretical studies have already explored this external enrichment channel across minihalos (Smith et al. 2015; Jeon et al. 2017; Hartwig et al. 2018). Assuming the gas in the neighboring system to be primordial, the abundance ratios of the supernova yields should largely remain preserved, such as the high $[\text{C}/\text{Fe}]$ ratio in combination with the low iron abundances, as well as enhanced $[\alpha/\text{Fe}]$ and $[\text{Zn}/\text{Fe}]$ values. Such a channel could have important implications for our understanding of the first chemical enrichment events and how these are preserved in second-generation UMP stars, especially those highly enhanced in carbon, such as the CEMP star HE 1327–2326.

An external enrichment scenario is principally supported by the outer halo nature of HE 1327–2326 and similar metal-poor stars (Tissera et al. 2014; Battaglia et al. 2017). As such, they are likely accreted from some smaller now disrupted system, such as a primordial minihalo. The accretion origin of HE 1327–2326 is based on its proper motion values from the latest *Gaia* DR2 kinematic parameters for proper motions ($\mu_{\text{RA}} = -52.52 \pm 0.04 \text{ mas yr}^{-1}$ and $\mu_{\text{DEC}} = 45.50 \pm 0.04 \text{ mas yr}^{-1}$) and parallax ($\pi = 0.887 \pm 0.023 \text{ mas}$) used with a Galactic dynamical model (Carollo et al. 2014; Frebel et al. 2018).

Stars such as HE 1327–2326 might then have actually formed in these externally enriched neighboring primordial systems long before those were accreted into the

Milky Way, as part of its own hierarchical growth. Future cosmological simulations will be able to provide additional insight into the nature of this channel, or provide alternative explanation for the formation sites of second-generation CEMP stars with the lowest [Fe/H] abundances.

We thank the anonymous referee for the careful reading of our manuscript and the insightful comments and suggestions. We also thank Arthur Choplin, Volker Bromm, John Wise, Britton Smith and Myoungwon Jeon for useful discussion. R.E., A.F., and I.U.R.

acknowledge generous support for program HST-GO-14151 provided by a grant from STScI, which is operated by AURA, under NASA contract NAS 5-26555. R.E., A.F., I.U.R. and V.P. acknowledge support from JINA-CEE, funded in part by the National Science Foundation under Grant No. PHY-1430152. A.F. is supported by NSF-CAREER grant AST-1255160. I.U.R. acknowledges additional support from NSF grants AST-1613536 and AST-1815403.

Software: MOOG (Snedden 1973; Sobeck et al. 2011), MULTI (Carlsson 1986, 1992), MARCS (Gustafsson et al. 1975, 2008)

REFERENCES

- Abohalima, A., & Frebel, A. 2018, *ApJS*, 238, 36
- Aoki, W., Frebel, A., Christlieb, N., et al. 2006, *The Astrophysical Journal*, 639, 897
- Asplund, M. 2005, *Annual Review of Astron and Astrophys*, 43, 481
- Asplund, M., Grevesse, N., Sauval, A. J., & Scott, P. 2009, *Annual Review of Astron and Astrophys*, 47, 481
- Barklem, P. S., Christlieb, N., Beers, T. C., et al. 2005, *Astronomy and Astrophysics*, 439, 129
- Battaglia, G., North, P., Jablonka, P., et al. 2017, *Astronomy & Astrophysics*, 608, A145
- Beers, T. C., & Christlieb, N. 2005, *Annual Review of Astronomy & Astrophysics*, 43, 531
- Bergemann, M., Lind, K., Collet, R., Magic, Z., & Asplund, M. 2012, *Monthly Notices of the RAS*, 427, 27
- Bessell, M. S., Collet, R., Keller, S. C., et al. 2015, *The Astrophysical Journal letters*, 806, L16
- Bromm, V., Yoshida, N., Hernquist, L., & McKee, C. F. 2009, *Nature*, 459, 49
- Burrows, A., Ott, C. D., & Meakin, C. 2004, in *Cosmic explosions in three dimensions*, ed. P. Höflich, P. Kumar, & J. C. Wheeler, 209
- Carlsson, M. 1986, *Uppsala Astronomical Observatory Reports*, 33
- Carlsson, M. 1992, in *Astronomical Society of the Pacific Conference Series*, Vol. 26, *Cool Stars, Stellar Systems, and the Sun*, ed. M. S. Giampapa & J. A. Bookbinder, 499
- Carollo, D., Freeman, K., Beers, T. C., et al. 2014, *The Astrophysical Journal*, 788, 180
- Casey, A. R. 2014, PhD thesis, Australian National University, doi:10.5281/zenodo.49493
- Castelli, F., & Kurucz, R. L. 2004, *astro-ph/0405087*
- Cayrel, R., Depagne, E., Spite, M., et al. 2004, *Astronomy & Astrophysics*, 416, 1117
- Choplin, A., Hirschi, R., Meynet, G., & Ekström, S. 2017, *Astronomy & Astrophysics*, 607, L3
- Choplin, A., Hirschi, R., Meynet, G., et al. 2018, *A&A*, 618, A133
- Christlieb, N., Gustafsson, B., Korn, A. J., et al. 2004, *The Astrophysical Journal*, 603, 708
- Cooke, R. J., & Madau, P. 2014, *The Astrophysical Journal*, 791, 116
- Ekström, S., Meynet, G., Chiappini, C., Hirschi, R., & Maeder, A. 2008, *Astronomy & Astrophysics*, 489, 685
- Ezzeddine, R., & Frebel, A. 2018, *The Astrophysical Journal*, 863, 168
- Ezzeddine, R., Frebel, A., & Plez, B. 2017, *The Astrophysical Journal*, 847, 142
- Fox, A. J., et al. 2015, "COS Data Handbook", STScI
- Frebel, A., Chiti, A., Ji, A. P., Jacobson, H. R., & Placco, V. M. 2015, *The Astrophysical Journal letters*, 810, L27
- Frebel, A., Collet, R., Eriksson, K., Christlieb, N., & Aoki, W. 2008, *The Astrophysical Journal*, 684, 588
- Frebel, A., Ji, A. P., Ezzeddine, R., et al. 2018, *ArXiv e-prints*, arXiv:1810.01228
- Frebel, A., & Norris, J. E. 2015, *Annual Review of Astron and Astrophys*, 53, 631
- Frebel, A., Aoki, W., Christlieb, N., et al. 2005, *Nature*, 434, 871
- Fröhlich, C., Martínez-Pinedo, G., Liebendörfer, M., et al. 2006a, *Physical Review Letters*, 96, 142502
- Fröhlich, C., Hauser, P., Liebendörfer, M., et al. 2006b, *ApJ*, 637, 415
- Fryer, C. L., & Heger, A. 2000, *The Astrophysical Journal*, 541, 1033

- Gaia Collaboration, Brown, A. G. A., Vallenari, A., et al. 2018, *A&A*, 616, A1
- Ghavamian, P., Aloisi, A., Lennon, D., et al. 2009, Preliminary Characterization of the Post- Launch Line Spread Function of COS, Tech. rep.
- Greif, T. H., Glover, S. C. O., Bromm, V., & Klessen, R. S. 2010, *The Astrophysical Journal*, 716, 510
- Grimmett, J. J., Heger, A., Karakas, A. I., & Müller, B. 2018, *Monthly Notices of the Royal Astronomical Society*, 479, 495
- Gustafsson, B., Bell, R. A., Eriksson, K., & Nordlund, A. 1975, *Astronomy and Astrophysics*, 42, 407
- Gustafsson, B., Edvardsson, B., Eriksson, K., et al. 2008, *Astronomy and Astrophysics*, 486, 951
- Hartwig, T., Bromm, V., Klessen, R. S., & Glover, S. C. O. 2015, *MNRAS*, 447, 3892
- Hartwig, T., Yoshida, N., Magg, M., et al. 2018, *Monthly Notices of the Royal Astronomical Society*, 478, 1795
- Heger, A., & Woosley, S. E. 2010, *The Astrophysical Journal*, 724, 341
- Hirai, Y., Saitoh, T. R., Ishimaru, Y., & Wanajo, S. 2018, *The Astrophysical Journal*, 855, 63
- Hollek, J. K., Frebel, A., Roederer, I. U., et al. 2011, *The Astrophysical Journal*, 742, 54
- Iwamoto, N., Umeda, H., Tominaga, N., Nomoto, K., & Maeda, K. 2005, *Science*, 309, 451
- Jacobson, H. R., Keller, S., Frebel, A., et al. 2015, *The Astrophysical Journal*, 807, 171
- Jeon, M., Besla, G., & Bromm, V. 2017, *The Astrophysical Journal*, 848, 85
- Joggerst, C. C., Almgren, A., Bell, J., et al. 2010, *The Astrophysical Journal*, 709, 11
- Keller, S. C., Bessell, M. S., Frebel, A., et al. 2014, *Nature*, 506, 463
- Korn, A. J., Richard, O., Mashonkina, L., et al. 2009, *The Astrophysical Journal*, 698, 410
- Maeda, K., & Nomoto, K. 2003, *The Astrophysical Journal*, 598, 1163
- Maeder, A., Meynet, G., & Chiappini, C. 2015, *A&A*, 576, A56
- Mashonkina, L., Gehren, T., Shi, J.-R., Korn, A. J., & Grupp, F. 2011, *Astronomy and Astrophysics*, 528, A87
- Meynet, G., Ekström, S., & Maeder, A. 2006, *Astronomy and Astrophysics*, 447, 623
- Nomoto, K., Kobayashi, C., & Tominaga, N. 2013, *Annual Review of Astronomy and Astrophysics*, 51, 457
- Nordlander, T., Amarsi, A. M., Lind, K., et al. 2017, *Astronomy and Astrophysics*, 597, A6
- Omukai, K., & Palla, F. 2001, *ApJL*, 561, L55
- Placco, V. M., Frebel, A., Beers, T. C., et al. 2016, *The Astrophysical Journal*, 833, 21
- Pruet, J., Hoffman, R. D., Woosley, S. E., Janka, H.-T., & Buras, R. 2006, *ApJ*, 644, 1028
- Roederer, I. U., & Barklem, P. S. 2018, *The Astrophysical Journal*, 857, 2
- Roederer, I. U., Placco, V. M., & Beers, T. C. 2016, *The Astrophysical Journal Letters*, 824, L19
- Smith, B. D., Wise, J. H., O'Shea, B. W., Norman, M. L., & Khochfar, S. 2015, *MNRAS*, 452, 2822
- Snedden, C. A. 1973, PhD thesis
- Snyder, E., & Sonnentrucker, P. 2017, "Analysis of the COS/NUV Extraction Box Heights", STScI
- Sobeck, J. S., Kraft, R. P., Sneden, C., et al. 2011, *The Astronomical Journal*, 141, 175
- Stacy, A., Bromm, V., & Loeb, A. 2011, *Monthly Notices of the Royal Astronomical Society*, 413, 543
- Stacy, A., Greif, T. H., & Bromm, V. 2012, *MNRAS*, 422, 290
- Takeda, Y., Hashimoto, O., Taguchi, H., et al. 2005, *Publications of the Astronomical Society of Japan*, 57, 751
- Thévenin, F., & Idiart, T. P. 1999, *The Astrophysical Journal*, 521, 753
- Tissera, P. B., Beers, T. C., Carollo, D., & Scannapieco, C. 2014, *Monthly Notices of the Royal Astronomical Society*, 439, 3128
- Tominaga, N. 2009, *The Astrophysical Journal*, 690, 526
- Tominaga, N., Maeda, K., Umeda, H., et al. 2007a, *The Astrophysical Journal Letters*, 657, L77
- Tominaga, N., Umeda, H., & Nomoto, K. 2007b, *The Astrophysical Journal*, 660, 516
- Tsujimoto, T., & Nishimura, N. 2018, *The Astrophysical Journal Letters*, 863, L27
- Umeda, H., & Nomoto, K. 2002, *The Astrophysical Journal*, 565, 385
- Woosley, S. E., & Weaver, T. A. 1995, *The Astrophysical Journal Supplementary Series*, 101, 181
- Yong, D., Norris, J. E., Bessell, M. S., et al. 2013, *The Astrophysical Journal*, 762, 27
- Yoshida, N., Omukai, K., Hernquist, L., & Abel, T. 2006, *ApJ*, 652, 6